Published in final edited form as:
J Comp Neurol. 2006 April 1; 495(4): 453–469. doi:10.1002/cne.20894.

SYNAPTIC MICROCIRCUITRY OF TYROSINE HYDROXYLASE-CONTAINING NEURONS AND TERMINALS IN THE STRIATUM OF MPTP-TREATED MONKEYS

Maney Mazloom[1] and **Yoland Smith**[1,2,*]

[1]Yerkes National Primate Research Center, Emory University, 954, Gatewood RD NE, Atlanta, GA 30322, USA

[2]Department of Neurology, Emory University, 954, Gatewood RD NE, Atlanta, GA 30322, USA

Abstract

A population of tyrosine hydroxylase (TH)-containing neurons that up-regulates after lesion of the nigrostriatal dopaminergic pathway has been described in the primate striatum. The goal of this study was to examine the morphology, synaptology and chemical phenotype of these neurons and TH-immunoreactive (TH-ir) terminals in the striatum of 1-methyl-4-phenyl-1,2,3,6-tetrahydropyridine (MPTP)-treated rhesus monkeys. TH-ir perikarya were small (10-12 μm), displayed nuclear invaginations and received very few synaptic inputs. On the other hand, TH-containing dendrites were typically large in diameter (>1.0 μm) and received scarce synaptic innervation from putative excitatory and inhibitory terminals forming asymmetric and symmetric synapses, respectively. More than 70% of TH-positive intrastriatal cell bodies were found in the caudate nucleus and the pre-commissural putamen, considered as the associative functional territories of the primate striatum. Less then 10% of these cells displayed calretinin immunoreactivity. TH-immunoreactive terminals rarely formed clear synaptic contacts, except for a few that established asymmetric axo-dendritic synapses. Almost two thirds of TH-containing boutons displayed GABA immunoreactivity in the striatum of parkinsonian monkeys whereas less than 5% did so in the normal striatum.

These findings provide a strong support for the existence of a population of putative catecholaminergic interneurons in the associative territory of the striatum in parkinsonian monkeys. Their sparse synaptic innervation raises interesting issues regarding synaptic and non-synaptic mechanisms involved in the regulation and integration of these neurons in the striatal microcircuitry. Finally, the co-expression of GABA in TH-positive terminals in the striatum of dopamine-depleted monkeys suggests dramatic neurochemical changes in the catecholaminergic modulation of striatal activity in Parkinson's disease.

Keywords

Dopamine; Parkinson; caudate nucleus; putamen; nigrostriatal degeneration

Parkinson's disease (PD) is characterized by the progressive degeneration of the dopaminergic nigrostriatal pathway (Ehringer and Hornykiewicz, 1960). Clinical symptoms, such as rigidity, akinesia and resting tremor, appear only following more than 70-80% loss of midbrain dopaminergic neurons in the substantia nigra pars compacta (SNc)

*Send correspondence to: Yoland Smith Yerkes Primate Center Emory University 954, Gatewood Rd NE Atlanta, GA 30322 USA Tel: (404) 727 7519 Fax: (404) 727 3278 Email: yolands@rmy.emory.edu

(Hornykiewicz and Kish, 1987; Kish et al., 1988), suggesting that important compensatory mechanisms are established while the neurodegeneration progresses (Bezard and Gross, 1998; Bezard et al., 2003). Parkinsonian symptoms can be induced in animal models by selective lesion of SNc neurons in rodents and non-human primates by administration of 6-hydroxydopamine (6-OHDA) and 1-methyl-4-phenyl-1,2,3,6-tetrahydropyridine (MPTP), respectively (Ungerstedt, 1968; Burns et al., 1983; Langston et al., 1983; Heikkila et al., 1984). A number of studies have indicated that a population of intrastriatal tyrosine hydroxylase (TH)-immunoreactive (ir) neurons increases dramatically in number following lesions of the SNc in rats, monkeys and humans (Dubach et al., 1987; Tashiro et al., 1989a,b; Mura et al., 1995; Betarbet et al., 1997; Porritt et al., 2000; Cossette et al., 2003, 2004), maybe as a compensatory reaction to the tremendous loss of striatal dopamine levels produced by nigral lesion. (Dubach et al., 1987; Tashiro et al., 1989a,b; Mura et al., 1995; Betarbet et al., 1997).

Although data gathered on the morphology and chemical phenotype of these intrastriatal neurons in rodents are quite variable among research groups (Tashiro et al., 1989a,b;Mura et al., 1995;Meredith et al., 1999,O'Byrne et al., 2000), results obtained in MPTP-treated monkeys regarding the distribution, morphology and neurotransmitter content of these neurons have been quite consistent (Dubach et al., 1987;Betarbet et al., 1997;Smith and Kieval, 2000). In brief, these cells are defined as small TH-immunoreactive aspiny neurons located along the dorsolateral border of the caudate nucleus and putamen (Dubach et al., 1987;Betarbet et al., 1997;Smith and Kieval, 2000). Co-localization studies in the striatum of MPTP-treated monkeys have shown that nearly all TH-ir striatal neurons express glutamate decarboxylase (GAD_{67}), but not parvalbumin and nitric oxide synthase, two markers of striatal interneurons (Kawaguchi et al., 1995;Betarbet et al., 1997). On the other hand, these neurons are immunoreactive for dopamine transporter (DAT) and the transcription factor Nurr1 suggesting that they very likely use dopamine as neurotransmitter (Betarbet et al., 1997;Cossette et al., 2004), an issue that is not so clear in rodents (Tashiro et al., 1989a,b;Mura et al., 1995;Meredith et al., 1999).

In order to elucidate the potential roles of these neurons in the primate striatum, a clear understanding of their synaptic microcircuitry is required. To address this issue, we performed an electron microscopic analysis of the ultrastructural features and synaptology of TH-ir neurons and tested the possibility of GABA co-expression in TH-positive terminals in the striatum of MPTP-treated rhesus monkeys.

Results of this study have been presented in abstract form (Mazloom et al., 2001).

MATERIALS AND METHODS

Animals and Preparation of Tissue

All animal use was in accordance with National Institutes of Health guidelines and was approved by the Emory University Institutional Animal Care and Use Committee. Six adult female rhesus monkeys were used in this study. Two normal monkeys were used as controls. Three monkeys received unilateral intracarotid injections of MPTP (Total dose: 0.6-0.9 mg/kg), which resulted in contralateral parkinsonian symptoms while the remaining animal was injected systemically (Total dose: 0.9 mg/kg), thereby, displayed bilateral parkinsonian symptoms. The monkeys with unilateral lesions were perfused 5 to 10 months after receiving MPTP injections whereas the bilaterally parkinsonian monkey survived 18 months following MPTP lesioning. After deep anesthesia with an overdose of pentobarbital (30 mg/kg, i.v.), the monkeys were perfusion-fixed with a cold oxygenated Ringer's solution and a fixative containing 4% paraformaldehyde and 0.1 % glutaraldehyde in phosphate buffer (PB; 0.1 M, pH 7.4). The brains were removed from the skull, sliced in 60μm-thick

transverse sections using a vibrating microtome and processed for the immunohistochemical localization of TH at the light and electron microscopic levels.

Primary antibodies

Three different commercially available primary antibodies were used in this study. The specificity of these antibodies has been well characterized through immunoblotting and pre-absorbtion experiments on brain tissue. The mouse monoclonal TH antibodies (Chemicon Intl, Temecula, CA; catalog # MAB318-Lot # 20100252) recognize specifically an epitope on the outside of the regulatory N-terminus of TH. Tyrosine hydroxylase purified from the PC12 pheochromocytoma cell line was used as immunogen to generate these antibodies (Wolf and Kapatos, 1989). On Western blot, it labels a single band with a molecular weight of 59-61 kDA, which corresponds to that estimated for TH. On the other hand, it does not react with other closely related catecholamine enzymes including dopamine-beta-hydroxylase, phenylalanine hydroxylase, tryptophan hydroxylase, dehydropteridine reductase, sepiapterin reductase and phenethanolamine-M-methyl-transferase (Chemicon International, Inc., Temecula). To further test the specificity of these antibodies on monkey brain tissue, striatal sections from both normal and MPTP-treated monkeys were incubated in solution from which primary TH antibodies have been replaced by pre-immune mouse serum while the rest of the procedure remained the same. These specificity tests resulted in a complete lack of immunolabeling in the striatum of both normal and MPTP-treated monkeys.

The anti-calretinin polyclonal antibodies (SWANT, Bellinzona, Switzerland; Code # 7699/4-lot # 18299) have been raised in rabbits by immunization with recombinant human calretinin (Schwaller et al., 1993). This antiserum does not cross-react with other calcium binding proteins as determined by its distribution in the brain and by immunoblots (Schwaller et al., 1993). The overall pattern of labeling generated with this antiserum is the same as that previously reported using other specific calretinin antibodies (Resibois and Rogers, 1992). Omission of the calretinin antibodies from the incubation solutions resulted in a total lack of immunolabeling in the normal and MPTP-treated monkey striatum.

The commercially available polyclonal GABA antiserum (Sigma —Aldrich; Saint Louis, MI; product number A 2052) used for the postembedding immunogold procedure (see below) has been raised in rabbits using GABA-BSA as the immunogen. The rabbit anti-GABA antibodies show positive binding with GABA and GABA-KLH and negative binding with BSA in dot blot assay (Sigma-Aldrich; Saint-Louis, MI). Additional specificity tests have been performed on monkey striatal tissue (see below).

TH Immunostaining

Light microscopy—A series of 16 sections through the rostrocaudal extent of the striatum and 6 sections through the substantia nigra, from each of the four MPTP-treated monkeys, were processed for light microscopic analysis of TH immunolabeling. Sections processed for light microscopy were pretreated with sodium borohydride (1% in phosphate buffered saline [PBS], 0.01 M, pH 7.4) for 20 minutes, and pre-incubated for 1 hour with 1% normal horse serum (NHS), 0.3% Triton X-100, and 1% bovine serum albumin (BSA) in PBS. They were then incubated overnight at room temperature in the same solution containing primary mouse anti-TH antibodies (1:1000; Chemicon Intl, Temecula, CA). The sections were then rinsed in PBS and incubated at room temperature for 90 minutes in the same solution containing biotinylated horse anti-mouse immunoglobulins G (IgGs) (1:200, Vector Laboratories, Burlingame, CA) followed by a 90-minute incubation in the avidin-biotin peroxidase complex (ABC; 1:100 dilution in PBS/1%BSA, Vector Laboratories). Then, sections were washed in PBS and TRIS buffers (0.05 M, pH 7.6) before a 10-minute

incubation in 3,3′-diaminobenzidine tetrahydrochloride (DAB, 0.025%; Sigma, St. Louis, MO), 0.01 M imidazole (Fisher Scientific, Pittsburgh, PA) and 0.005% hydrogen peroxide. The reaction was stopped by repeated washes in PBS, sections were mounted on gelatin-coated slides, dehydrated, and a coverslip was applied with Permount. Sections were examined with a Leica DMRB microscope (Leica Microsystems, Inc., Bannockburn, IL), and images were acquired with a CCD camera (Leica DC500) controlled by Leica IN50 software.

Electron microscopy—Sections processed for electron microscopy were cryoprotected in 25% sucrose and 10% glycerol for 20 minutes before being frozen at -80°C for 20 minutes. They were then thawed and transferred for 5 minutes each in graded decreasing concentrations (80%, 60%, 30%, 15%) of cryoprotectant diluted in PBS. After being washed in PBS, the sections were processed for TH immunostaining the same way as for light microscopy, except that Triton X-100 was not used, and the incubation in primary antisera lasted 48 hours at 4°C.

TH/Calretinin co-localization—Fifteen sections of pre-commissural striatum collected from three monkeys were processed for this part of the study. They were first incubated for 20 minutes in sodium borohydride , thoroughly washed in PBS and then pre-incubated for 1 hour at room temperature in a mixture of 5% normal donkey serum (NDS; Jackson Immuno Lab; West Grove, PA), 1% BSA and 0.3% Triton-X-100 in PBS. This was followed by an overnight incubation at room temperature in a cocktail of rabbit anti-calretinin (1:15 000; SWANT, Switzerland) and mouse anti-TH (1:1000; Chemicon) diluted in PBS containing 1% NDS/1% BSA. The sections were then rinsed in PBS for 20 minutes and transferred for 1 hour at room temperature into a cocktail of FITC-conjugated donkey anti-rabbit IgGs (Jackson Immuno Lab; West Grove, PA) and TRITC-conjugated donkey anti-mouse IgGs (Jackson Immuno Lab; West Grove, PA) diluted 1:100 in PBS/1%NDS/1%BSA. After three 5-minute rinses in PBS, sections were placed into a solution of cupric sulfate/ammonium acetate (pH 5.0) for 30 minutes. They were then mounted on slides, coverslipped with Vectashield, sealed with nail polish and observed with a Leica DMRB light microscope (Leica Microsystems, Inc., Bannockburn, IL, USA) equipped with bandpass emission filters for FITC (510-525 nm) and TRITC (575-640 nm).

Processing of tissue for electron microscopy

The sections prepared for electron microscopy were washed in PB (0.1 M, pH 7.4) before post-fixation in 1% osmium tetroxide in PB for 20 minutes. They were then washed in PB (0.1 M, pH 7.4) and dehydrated in a graded series of alcohol and propylene oxide. 1% uranyl acetate was added to the 70% ethanol to improve the contrast of the tissue at the electron microscope. The sections were then embedded in resin (Durcupan; ACM, Fluka, Buchs, Switzerland) for 12 hours, mounted on microscope slides and placed in a 60°C oven for 48 hours. After examination at the light microscope, regions of interest from the striatum were cut out from the slides and glued on top of resin blocks with cyanoacrylate glue. Ultrathin 60-nm thick sections were cut with an ultramicrotome (Ultracut T2; Leica) and collected on Pioloform-coated single slot copper and gold grids. Sections collected on copper grids were stained with lead citrate (Reynolds, 1963) and examined with a Zeiss EM10C electron microscope whereas sections collected on gold grids were processed for the post-embedding immunogold localization of GABA within TH-ir terminals.

Post-embedding GABA immunocytochemistry

The protocol for post-embedding immunochemistry has been previously described (Somogyi et al., 1985; Phend et al., 1992). Briefly, ultrathin sections collected on gold grids were pre-incubated in TRIS-buffered saline (TBS; 0.05 M, pH 7.6) containing 0.01% Triton

X-100 for 10 minutes. Next, the sections were incubated overnight at room temperature in the same solution containing the primary rabbit anti-GABA antiserum (1:5000; Sigma, St Louis, MO). They were then rinsed in TBS/0.01% Triton X-100 (2 × 10 minutes, 1 × 30 minutes) and TBS (0.05 M, pH 8.2) for 10 minutes and incubated in a secondary antibody solution containing 15 nm gold-conjugated goat anti-rabbit (1:50 dilution) in TBS (0.05 M, pH 8.2) for 90 minutes. The sections were then washed in distilled water for 5 minutes, incubated in 1% aqueous solution of uranyl acetate for 90 minutes, and then washed in distilled water again for 5 minutes. From here, the sections were stained with lead citrate (Reynolds, 1963) and examined with a Zeiss EM10C electron microscope.

The specificity of labeling was tested by incubation in solutions from which the primary antiserum was replaced by pre-immune serum (Jackson Immuno. Laboratories, West Grove, PA). The tissue was completely devoid of gold particles following this incubation. In addition, the fact that gold particles labeling was largely confined to terminals forming symmetric synapses and that the overall pattern of labeling described in this study is consistent with that found in previous rodent studies using other specific GABA antibodies (Fujiyama et al., 2000) further support the specificity of this antiserum for GABA. Furthermore, specific GABA labeling was found in other brain regions with this antiserum (Watson and Bazzaz, 2001).

Analysis of Material

Image acquisition for electron microscopy—Electron micrographs were acquired with a CCD camera (Dual View 300W; Gatan, Inc., Pleasanton, CA) controlled by the DigitalMicrograph software (version 3.6.5; Gatan Inc.). Some digitally acquired micrographs were adjusted only for brightness and contrast, with the image resolution kept constant, with either DigitalMicrograph or Photoshop software (version 7.0; Adobe Systems, Inc., San Jose, CA) to optimize the quality of the images for analysis.

Distribution of TH-immunoreactive neurons—To illustrate the distribution of TH-immunoreactive (TH-ir) cells through the rostrocaudal extent of the striatum, the series of sections processed for light microscopy in each of the four MPTP-treated monkeys was examined using the Virtual Slice module of Neurolucida (Microbrightfield, Colchester, VT). The borders of the nuclei of interest (caudate and putamen) were outlined from a live image using a 2.5× objective and the entire area of these nuclei was examined at higher magnifications (10× objective) for TH-ir cell bodies. The images were then exported to Neuroexplorer (Microbrightfield) to determine the cross-sectional areas of the nuclei and the relative densities of TH-immunoreactive cells within each nucleus throughout the striatum.

Co-localization TH/CR in the striatum—To determine the degree of TH/CR co-localization, double immunostained striatal sections were scanned under the fluorescence microscope for TH-positive cell bodies (TRITC-labeled). Images (magnification 20X) of TH-immunoreactive neurons were acquired with a CCD camera (Leica DC500) controlled by Leica IM50 software (version 1.20). The same area was then examined using the emission filter for FITC to verify whether the TH-labeled neurons also displayed CR immunoreactivity. The percentage of single and double labeled neurons was then calculated for each animal.

EM Analysis of TH-ir Neurons—Two MPTP-treated animals were used for electron microscopic analysis. Blocks were selected from regions with the highest density of immunoreactive cell bodies and fibers. Whenever possible, ultrathin sections were collected serially with up to 6 sections per grid, and immunoreactive elements were examined in serial sections. In the electron microscope, sections were scanned in a non-random manner to

ensure that every TH-positive element within an ultrathin section would be examined. Labeled elements were categorized as: (1) terminals if they contained synaptic vesicles, or (2) dendrites if they contained microtubules or endoplasmic reticulum and were devoid of synaptic vesicles. The size, morphology, and pattern of synaptic inputs of TH-ir cell bodies and dendrites were determined. Negatives of TH-ir elements were scanned using a Hewlett Packard ScanJet 6300c and imported into the Neurolucida software to measure the diameter of labeled cell bodies and dendrites. The ultrastructural features of axon terminals in contact with TH-immunoreactive neurons were characterized, and the length of the active zones of all synapses onto TH-containing elements was measured in single ultrathin sections. The TH-ir terminals were ultrastructurally characterized, analyzed for any visible synapses and subsequently examined to determine the nature of their post-synaptic targets.

GABA/TH Co-localization—Four MPTP-treated animals and two control animals were used for the post-embedding analysis of GABA localization in TH-ir terminals. To determine whether TH-ir boutons displayed GABA immunoreactivity, the density of gold particles in terminals containing TH immunoreactivity was compared with the density of particles in TH-negative boutons forming symmetric (putative GABAergic) or asymmetric (putative glutamatergic) synapses. The quantification of immunogold labeling was performed as follows: Ultrathin sections were scanned at the electron microscope for the presence of TH-containing terminals. Photomicrographs of labeled boutons were taken and each negative was scanned and imported into image analysis software as described above. Cross-sectional areas of each terminal were measured and the relative density of gold particles within labeled and unlabelled terminals was determined. In MPTP-treated monkeys, immunogold-containing terminals were divided into two categories, namely the TH-ir terminals and boutons forming asymmetric synapses. To account for any variability between post-embedding incubations on different grids in MPTP-treated monkeys, each grid was analyzed separately and then the relative density of gold particles for all grids was normalized and pooled. The normalized values from each category of terminals from four grids of striatal tissue in MPTP-treated monkeys were plotted on distribution histograms and compared statistically with analysis of variance. In the control monkeys, immunogold containing terminals were divided into three categories: (1) TH-ir terminals, (2) TH-immunonegative terminals forming asymmetric synapses and (3) putative GABAergic TH-immunonegative terminals. The latter category was characterized by the presence of either a visible symmetric synapse or the pleomorphic appearance of large synaptic vesicles. The density values were taken from one grid and normalized. These values were then plotted on a histogram and compared statistically using analysis of variance and a Scheffe post-hoc comparison.

RESULTS

Light microscopic characterization of TH-ir neurons

Initially, TH-immunostained sections were examined at low magnification to determine the extent of the dopaminergic fiber loss in the striatum of MPTP-treated monkeys. Overall, the pattern of degeneration of TH-immunoreactive cells in the ventral midbrain and TH-containing fibers in the striatum was quite similar for the four MPTP-treated monkeys used in this study. As shown in Figure 1, there was a tremendous dopaminergic denervation of the dorsal striatum on the lesioned side compared to the control side in unilateral MPTP-lesioned animals (Fig. 1C, D). On the other hand, the TH innervation of the nucleus accumbens was relatively spared by the MPTP lesion (Fig. 1D). Correspondingly, the loss of TH-containing neurons in the ventral midbrain was more pronounced in the SNc, the main source of dopaminergic fibers to the dorsal striatum, than the ventral tegmental area (VTA), which contributes most of the dopaminergic innervation of the nucleus accumbens (Fig. 1A,

B). When examined at higher magnification, TH immunoreactivity was found in cell bodies and varicose processes in the caudate nucleus and putamen of both the unilateral (N=3) and bilateral (N=1) MPTP-lesioned animals (Fig. 2). In the three unilaterally lesioned monkeys, intrastriatal TH-immunoreactive neurons were found only on the side ipsilateral to the intracarotid MPTP injection, while both dorsal striata contained labeled neurons in the animal with bilateral nigrostriatal dopaminergic lesion. It is noteworthy that TH-positive neuronal cell bodies were not found in the ventral and dorsal striata of the two normal monkeys used in this study. The TH-containing neurons in the striatum of MPTP-treated monkeys had a small sized perikaryon (10-12 μm in diameter) with two or three dendritic trunks that gave rise to a variable number of smooth aspiny dendrites (Fig 2C, D).

Overall, the pattern of distribution of TH-immunoreactive neurons was the same for the four MPTP-treated monkeys used in this study. More than two thirds of these cell profiles were found in the caudate nucleus and the pre-commissural putamen (Fig. 3), considered as associative functional territories of the primate striatum (Parent, 1990). Figure 3 shows the localization of TH-containing cell bodies through the rostrocaudal extent of the striatum in one of the unilateral MPTP-treated monkeys. Although labeled neurons in the rostral caudate nucleus were homogeneously distributed, TH-ir neurons in the pre-commissural putamen were particularly abundant along its lateral border (Fig. 3-sections S3,S5). At post-commissural levels, neurons were primarily localized in the dorsolateral part of both structures (Fig. 3-sections S9,S12). It is important to note that TH-ir neurons and processes were also seen in the white matter overlying the striatum (Fig. 2A, B), but only cells localized within striatal borders were considered for the quantitative measurements shown in Figure 3.

Co-localization TH/CR

Overall, the pattern of distribution of TH-immunoreactive cell bodies in the double immunostained material was the same as that described above using the immunoperoxidase method. Similarly, numerous CR-positive cell bodies and varicose processes were found throughout the full extent of the striatum in a pattern similar to that previously described in squirrel monkeys (Prensa et al., 1998; Sidibe and Smith, 1999; Wu and Parent, 2000). Of a total of 49 TH-positive neuronal cell bodies (23 from MR38; 20 from MR 41 and 6 from MR 51) tested for CR immunoreactivity, only four (ie about 8%) were double labeled (Fig. 4 A1-A2). These four neurons were located in the rostralmost section (level corresponding to S5 in Figure 3) of the putamen in MR38 (N=3) and MR41 (N=1). All other TH-containing cells examined were devoid of CR immunoreactivity (Fig. 4 B1-B2).

Electron microscopic (EM) analysis of TH-ir neuronal elements

Analysis of striatal tissue from MPTP-treated monkeys prepared for electron microscopy yielded the same results. At the electron microscopic level, TH-ir cell bodies, dendrites and terminals showed strong immunostaining (Figs. 5-7). Occasionally, TH-containing myelinated and unmyelinated axons were seen, but their frequency was far lower than that of labeled dendrites and terminals. Similarly, only two immunoreactive spines were observed in all sections examined. The DAB deposit onto labeled elements (especially terminals) was, in some instances, extremely dense which made clear visualization, recognition of the boundaries, and type of synaptic specializations difficult to determine (Figs 7-8).

TH-ir cell bodies—Fifteen TH-ir cell bodies were identified and analyzed at the electron microscopic level. The DAB deposit was homogeneously distributed throughout the cytoplasm, but the nucleus was devoid of immunoreactivity (Fig. 5). In every perikarya examined, the nuclear membrane was deeply invaginated, a major ultrastructural feature of

striatal interneurons (Difiglia et al., 1980). In line with the light microscopic observations, cell bodies were small, ranging from 10 to 12 μm in diameter, and the shape was typically round or oval (Fig. 5). In general, immunoreactive perikarya received very few synaptic inputs. For instance, of the 15 cell bodies examined, only one axo-somatic asymmetric synapse was identified (Fig. 6D).

TH-ir dendrites—TH-ir dendrites were typically large in diameter (> 1.0 μm). Dendritic elements smaller than 0.5 μm were not found at the EM level (Table 1). The synaptic innervation of 205 TH-containing dendrites was examined. Overall, they received very sparse synaptic input (Table 1). Quantification of the total length of dendritic membrane contacted by synapses revealed that less than 1-2% of the total dendritic surface received synaptic inputs from boutons forming asymmetric (0.8%) or symmetric (0.2%) synapses (Table 2). Two different populations of terminals formed asymmetric synapses with TH-ir dendrites. The majority (17/22) comprised terminals with densely packed small, round, clear electron-lucent vesicles and a few dense core vesicles (Fig. 6B). A second population (5/22) consisted of terminals with a low density of large pleomorphic vesicles aggregated primarily at the active zone (b2 in Fig. 6A). On the other hand, the majority of boutons (6/8) forming symmetric synapses morphologically resembled the terminal "b1" depicted in Fig. 6A, i.e. they contained a large number of pleomorphic electron lucent vesicles and a few dense core vesicles homogeneously distributed throughout the terminal. A few axonal processes, which contained a small pool of pleomorphic electron lucent vesicles confined to the active zones, also formed "*en passant*" type symmetric synapses with TH-positive dendrites (Fig. 6C).

TH-ir terminals—The TH-ir terminals were often very intensely labeled making the ultrastructural features and type of synaptic specializations associated with them difficult to characterize (Figs. 7-8). Of the 82 terminals examined, 6 (7.3%) formed clear asymmetric synapses with small dendritic profiles (Fig. 7A, B). Five of these boutons were medium-sized (0.8-1.5 μm in diameter), packed with synaptic vesicles, contained one or two mitochondria and contacted unlabeled dendrites (Fig. 7A). The other terminal of this group was morphologically different, contained a much lower density of sparsely distributed synaptic vesicles and contacted a TH-positive dendrite (Fig. 7B). However, more than 90% of TH-containing terminals did not form clear synaptic contacts in the plane of section examined. As shown in Figure 8, synaptic specializations were hard to visualize even when the bouton was observed through many serial sections (Fig. 8A-F). There were some cases where the TH-containing terminals were apposed to unlabeled boutons, which, in turn, established asymmetric axo-spinous synapses (Fig. 7C-E).

GABA in TH-positive terminals—In order to characterize the phenotype of TH-containing terminals in the striatum of parkinsonian monkeys, we processed TH-immunostained striatal tissue from two normal and four MPTP-treated monkeys for the postembedding immunogold localization of GABA. Overall, the pattern of TH immunoreactivity in normal monkeys was the same as reported in previous monkey studies using either TH or dopamine antibodies (Arsenault et al. 1988; Lavoie et al., 1989). In GABA-immunostained sections, variable densities of gold particles overlaid pre- and postsynaptic striatal elements. To further assess the specificity of the GABA immunostaining generated in the tissue, the density of gold particles over putative glutamatergic terminals was measured and compared with that of unlabeled boutons forming symmetric synapses and TH-containing terminals. As shown in Figs. 9-10, the majority of TH-immunoreactive vesicle-filled profiles examined in the striatum of MPTP-treated monkeys displayed a significantly higher level of immunogold labeling than that associated with unlabeled boutons forming asymmetric synapses (analysis of variance, $p<0.0001$), but not significantly different from putative GABAergic terminals forming symmetric synapses

(p>0.3) (Figs. 9A-C; 10B). In contrast, TH-ir terminals displayed the same low level of immunogold labeling as unlabeled terminals forming asymmetric synapses in the striatum of the normal monkey (p>0.9) (Figs 9D; 10A). The density of gold particles associated with these two sets of terminals was significantly lower (p<0.001) than the level of immunogold labeling measured in putative GABAergic boutons (Fig. 9D, 10A). To determine the percentages of TH-ir terminals that co-express GABA, we used an arbitrary criterion that TH-positive terminals with a density of gold particles three times higher than the average density of labeling associated with putative glutamatergic terminals would be considered GABAergic. Using this quantitative approach, we found that 68% of TH-containing terminals in the striatum of MPTP-treated monkeys co-express GABA whereas only 4% do so in the normal striatum (Fig. 10). None of the 82 TH-containing terminals examined in the MPTP-treated monkeys formed clear synaptic contacts.

DISCUSSION

The findings of the present study provide a detailed description of the distribution and ultrastructural features of TH-ir neurons and terminals in the striatum of MPTP-treated monkeys. Five main conclusions can be drawn from our observations: (1) Intrastriatal TH-containing cells belong to a homogeneous population of small-sized neurons with aspiny dendrites that display the ultrastructural features of striatal interneurons. However, less than 10% of them displays CR immunoreactivity, one of the markers of striatal interneurons. (2) These neurons are largely confined to the pre-commissural putamen and caudate nucleus, considered as the associative territory of the primate striatum. (3) They receive very sparse synaptic innervation from putative inhibitory and excitatory terminals that form axo-dendritic symmetric and asymmetric synapses, respectively. (4) TH-immunoreactive terminals in the dorsal striatum of MPTP-treated monkeys rarely form clear synaptic contacts, except for a few asymmetric axo-dendritic synapses. (5) More than two thirds of TH-positive terminals in the striatum of MPTP-treated monkeys display GABA immunoreactivity, whereas less than 5% of TH-positive boutons do so in the normal striatum.

Together, these observations raise interesting questions regarding the morphology, synaptic regulation, distribution and chemical phenotype of TH-containing neurons in the striatum of parkinsonians. In the following account, these issues will be addressed, the potential origin of these neurons will be discussed and hypotheses about their therapeutic relevance in Parkinson’s disease will be examined.

Phenotype of TH-ir cells in rats and primates

In primates, more than 90% of intrastriatal TH-ir neurons have been described by various groups as being morphologically similar to striatal interneurons. However, data from different rodent models of Parkinson’s disease resulted in a greater level of variability in the relative abundance and morphological phenotype of intrastriatal TH-positive neurons. For instance, TH- and aromatic L-amino acid decarboxylase (AADC)-ir neurons were first observed in normal rat striatum and subsequently found to increase after 6-OHDA lesions of the nigrostriatal pathway in rats (Tashiro et al., 1989a,b). Initially, these cells were categorized as medium sized spiny neurons that co-express TH and AADC immunoreactivity (Tashiro et al., 1989a,b). However, recent studies indicated that TH and AADC might, in fact, be segregated into distinct neuronal populations with different morphology and location (Mura et al., 1995;Meredith et al., 1999). The AADC-ir neurons were subsequently characterized as small and aspiny, reminiscent of striatal interneurons (Mura et al., 1995). A population of striatal dopamine-immunoreactive cells, morphologically similar and distributed according to the same pattern as AADC-ir neurons, was recently found in the dorsomedial striatum of 6-OHDA-lesioned rats (Meredith et al.,

1999). According to these data, the dopamine- and AADC-containing neurons are distinct from TH-ir neurons which were defined as medium sized, spiny and localized primarily in the ventral striatum (Meredith et al., 1999). However, O'Byrne et al. (2000) identified a population of TH-ir neurons that receive inputs and morphologically resemble striatal interneurons in the striatum of MPP+-treated rats. Finally, Lopez-Real et al. (2003) identified two populations of TH-ir neurons in the dopamine-denervated dorsal striatum of rats and categorized them as bipolar/middle sized/aspiny cells or multipolar/spiny neurons (Lopez-Real et al., 2003). Interestingly, some studies were unable to locate any TH-ir neurons in the lesioned or normal rat striatum (Dubach et al., 1987;Betarbet et al., 1997). The use of different animal models, post-lesion survival time and variable degree of lesion-induced striatal dopamine depletion may account for some of these discrepancies.

Our findings are largely consistent with previous monkey and human studies, although some noticeable differences are worth some consideration. Although all primate studies, including ours, demonstrated that the vast majority of intrastriatal TH-immunoreactive neurons in the dopamine-denervated striatum display the ultrastructural and morphological features of interneurons (Dubach et al., 1987; Betarbet et al., 1997; O'Byrne et al., 2000; Porritt et al., 2000; Smith and Kieval, 2000; Cossette et al., 2004, 2005), previous findings from normal and parkinsonian humans and monkeys have also described a small subset of large multipolar spiny neurons (Betarbet et al., 1997; Cossette et al., 2005). We could not find such neuronal subtypes in our material. Various factors could be considered as potential explanations for this discrepancy including the age of monkeys and humans used if the different studies, postmortem delays of human brain tissue, variability in the sampling strategies among studies, extent of TH immunostaining in distal dendrites, variable drug therapies between animal and human subjects, etc… In addition, it is noteworthy that spines are highly dynamic structures that are endowed with tremendous capabilities in responding to behavioral, neurochemical or environmental changes by excessive growth or retraction from the dendritic tree (Harris and Kater, 1994; Ingham et al., 1998). Another difference between our findings and those from previous primate studies is the fact that we could not find any TH-positive neurons in the normal striatum, while a small, but significant, number of such neurons has been described by other investigators in normal humans and monkeys (Dubach et al., 1987; Betarbet et al., 1997; Porritt et al., 2000; Cossette et al., 2004, 2005). The strong TH-immunoreactive neuropil in the striatum of control monkeys might have obscured the detection of these neurons in our material at the light microscopic level. However, it is noteworthy that a small proportion of TH-immunoreactive vesicle-filled profiles expressed GABA immunoreactivity in the normal striatum, suggesting the possibility that a small subset of intrastriatal TH/GABA-positive boutons might arise from intrinsic neurons, even in normal monkeys.

Previous co-localization studies with markers of striatal interneurons (parvalbumin, nitric oxide synthase) were unsuccessful in characterizing the precise phenotype of TH-positive striatal neurons (Betarbet et al., 1997). Our findings extend these observations, showing that less than 10% of TH-positive cell bodies expressed CR immunoreactivity in the anterior striatum of MPTP-treated monkeys. Together, these findings suggest that the TH-containing neurons visualized in the primate striatum after dopaminergic depletion are either newly generated cells or a subset of pre-existing interneurons that up-regulate its TH expression as a compensatory mechanism for the dramatic loss of striatal dopamine (Yang et al., 2002; Cossette et al., 2004).

Synaptic inputs onto TH-ir dendrites

One of the main ultrastructural features of intrastriatal TH-positive neurons is their scarce synaptic innervation made up of putative excitatory and inhibitory terminals. Although various interneurons (Chang and Kita, 1992; Vuillet et al., 1992; Morello et al., 1997) or

extrinsic inputs (Parent, 1990; Lapper et al., 1992; Sadikot et al., 1992a,b; Bennett and Bolam, 1994; Rudkin and Sadikot, 1999; Sidibe and Smith, 1999; Thomas et al., 2000) could be suggested as potential sources of this innervation, anterograde labeling is essential to clearly assess the exact origin of synaptic inputs to these cells. Because of the lack of quantitative information on their degree of synaptic innervation, it is hard to compare the pattern of innervation of TH-immunoreactive neurons described in this study with that of other populations of striatal interneurons. However, the qualitative description of the degree of synaptic innervation of cholinergic (DiFiglia, 1987), parvalbumin-immunoreactive (Lapper et al., 1992; Bennett and Bolam, 1994) and calretinin-containing (Bennett and Bolam, 1993) interneurons suggest a larger density of axo-somatic and axo-dendritic synapses on the surface of the neurons compared to intrastriatal TH-containing neurons.

The sparse synaptic innervation of these neurons raise the interesting possibilities that they may not be regulated in a typical synaptic fashion or perhaps necessitate very little synaptic inputs to maintain their basal activity. For instance, cytokines and diffusible molecules such as nitric oxide regulate activity of other monoaminergic neurons through nonsynaptic mechanisms (Schulman, 1997; Vizi and Kiss, 1998; Vizi, 2000; Szelenyi, 2001). One must also consider the alternative hypothesis that TH-ir neurons may be regulated by typical neurotransmitters in a nonsynaptic manner. A growing body of literature, indeed, suggests that most neurotransmitters released by axon terminals with or without synaptic contacts can mediate their effects upon activation of extrasynaptic receptors (Agnati et al., 1986, 1995a,b, 2000; Isaacson et al., 1993; Zoli and Agnati, 1996; Zoli et al., 1999; Rusakov and Lehre, 2002). Finally, these intrastriatal TH-ir neurons may be a novel population of immature cells that do not receive a full complement of synaptic inputs. To gain a better understanding of the mechanisms that modulate the activity of these neurons, detailed immunocytochemical and electrophysiological studies of the localization and functions of various neurotransmitter receptor subtypes expressed by these cells should be conducted.

TH-ir terminals and colocalization with GABA

One of the main findings of this study is that most TH-immunoreactive terminals in the striatum of parkinsonian monkeys display GABA immunoreactivity. In contrast, TH-positive terminals in the striatum of normal monkeys are largely devoid of GABA. Together with the previous finding that all intrastriatal TH-positive neurons in the striatum of MPTP-treated monkeys display GAD67 immunolabeling (Betarbet et al., 1997), these observations suggest that, at least, a subset of TH/GABA-positive terminals in the striatum of parkinsonian monkeys may arise from intrinsic TH/GABA-containing interneurons. However, another interesting possibility is that some of these boutons originate from sprouted axons of the remaining SNc neurons. The formation of new branches or sprouting is, indeed, one of the mechanisms used by nigrostriatal neurons to compensate for partial dopaminergic lesion in animal models of Parkinson's disease (Song and Haber, 2000; Stanic et al., 2003a,b). Interestingly, the ultrastructural features of anterogradely labeled boutons in the striatum of rats with partial dopaminergic lesion resemble those of TH-immunoreactive terminals described in the present study (Stanic et al., 2003a). However, since the chemical phenotype of the anterogradely labeled SNc boutons has not been characterized in Stainic et al (2003a) study, great care must be taken in comparing these findings with our data. The degree of TH/GABA co-localization in the remaining dopaminergic SNc neurons that survive partial lesion of the nigrostriatal pathway should be examined to further address this issue.

GABA co-localization with TH in the striatum may have interesting functional implications. For instance, GABA and markers of catecholamines co-localize and play important regulatory functions in other neuronal systems of various vertebrate and invertebrate species (Gall et al., 1987; Campbell et al., 1991; Nguyen-Legros et al., 1997; Dunker, 1998; Diaz-

Rios et al., 2002; Andrade da Costa and Hoko, 2003). Interestingly, a recent in vitro study demonstrated a direct functional coupling between the dopamine receptor D5 and the GABA-A receptor subunit, gamma 2 (Liu et al., 2000). Although the exact significance of the GABA/TH co-localization described in the present study remains unclear, these observations pave the way for multifarious and complex effects the co-release of GABA and catecholamines may exert on their postsynaptic targets in the striatum of parkinsonians. A common feature of most TH-immunoreactive terminals examined in the striatum of MPTP-treated monkeys is their low incidence of clear synaptic contacts. However, this might be due to technical limitations inherent to the fact that these boutons displayed very robust peroxidase labeling making difficult the analysis and categorization of synaptic specializations established by these terminals. On the other hand, non-synaptic release of catecholamines from these terminals must also be considered, as was previously reported for dopamine in the normal rat striatum (Descarries et al., 1996; Agnati and Fuxe, 2000; Descarries and Mechawar, 2000; Pickel, 2000; Rice, 2000). The fact that dopamine receptors in striatal neurons are predominantly extrasynaptic strongly support this possibility (Sesack et al., 1994; Hersch et al., 1995; Yung et al., 1995; Pickel, 2000).

Localization of TH-ir neurons within the striatum

The present study indicates that TH-ir neurons are primarily localized in the associative areas of the striatum, namely the pre-commissural putamen and caudate nucleus (Parent, 1990). Interestingly, studies of the clinical manifestation of Parkinson's disease have indicated that cognitive deficits and dementia, symptoms of Parkinson's disease related to the associative areas of the striatum, arise much later than the typical motor symptoms in humans (Watts and Koller, 1997). One may, therefore, speculate that the localization of TH-ir neurons in the associative striatum act as compensatory mechanisms that delay the onset of cognitive deficits in parkinsonian patients. However, it is important to note that other studies have suggested that cognitive symptoms appear either earlier or concurrent with the motor deficits in Parkinson's disease dependent on many factors including the age of onset of the disease (Schneider and Kovelowski, 1990; Levin and Katzen, 1995). Although the potential compensatory roles of these neurons remain to be clearly established, the selective accumulation of these cells into associative striatal regions surely deserves consideration while addressing this issue in future studies.

Concluding Remarks

Although our findings provide interesting and critical information on the anatomical substrate that underlie the regulation and functions of intrastriatal TH-immunoreactive neurons, various questions remain unanswered regarding this intriguing neuronal population. One obvious issue to address is to determine the exact origin of these neurons in the brains of parkinsonians. While their morphologic characteristics are consistent with those of pre-existing striatal interneurons (see above), there is no direct evidence to support this claim. Another possibility is that they belong to a population of newly generated neurons that migrate to the striatum in response to dopamine depletion (Cossette et al., 2004). Although it remains a highly controversial issue for the cerebral cortex (Rakic, 2002), neurogenesis in the dentate gyrus of the hippocampus and the subventricular zone in adult rats, monkeys, and humans is well established (Cameron et al., 1993; Doetsch et al., 1997; Eriksson et al., 1998; Gould et al., 1999a,b; Bernier et al., 2000). Furthermore, new neurons have been identified in the adult striatum after middle cerebral artery occlusion (Arvidsson et al., 2002; Parent et al., 2002). These observations, combined with those from a recent study showing that administration of glial derived neurotrophic factor (GDNF) dramatically increase the number of TH-containing neurons in the striatum of aged and MPTP-treated monkeys (Palfi et al., 2002), raise very exciting possibilities for the development of novel therapeutic

strategies aimed at stimulating the development and growth of these neurons in parkinsonians.

Acknowledgments

This work was supported by NIH grants P50 NS38399-01 to YS and the Yerkes Center base grant RR 00165.

REFERENCES

Agnati LF, Bjelke B, Fuxe K. Volume versus wiring transmission in the brain: a new theoretical frame for neuropsychopharmacology. Med Res Rev. 1995a; 15:33–45. [PubMed: 7898168]

Agnati LF, Fuxe K. Volume transmission as a key feature of information handling in the central nervous system: possible new interpretative value of the Turing's B-type machine. Prog Brain Res. 2000; 125:3–19. [PubMed: 11098650]

Agnati LF, Fuxe K, Zoli M, Ozini I, Toffano G, Ferraguti F. A correlation analysis of the regional distribution of central enkephalin and beta-endorphin immunoreactive terminals and of opiate receptors in adult and old male rats. Evidence for the existence of two main types of communication in the central nervous system: the volume transmission and the wiring transmission. Acta Physiol Scand. 1986; 128:201–207. [PubMed: 3022556]

Agnati LF, Zoli M, Ferrari R, Di Paola L, Torri C, Fuxe K, Zini I. Evidence for the existence of pulses of dopamine in the extracellular space of the rat striatum. Prog Brain Res. 2000; 125:303–308. [PubMed: 11098666]

Agnati LF, Zoli M, Stromberg I, Fuxe K. Intercellular communication in the brain: wiring versus volume transmission. Neuroscience. 1995b; 69:711–726. [PubMed: 8596642]

da Costa, BL Andrade; Hoko, JN. Coexistence of GAD-65 and GAD-67 with tyrosine hydroxylase and nitric oxide synthase in amacrine and interplexiform cells of the primate, Cebus apella. Vis Neurosci. 2003; 20:153–163. [PubMed: 12916737]

Arvidsson A, Collin T, Kirik D, Kokaia Z, Lindvall O. Neuronal replacement from endogenous precursors in the adult brain after stroke. Nat Med. 2002; 8:963–970. [PubMed: 12161747]

Arsenault MY, Parent A, Seguela P, Descarries L. Distribution and morphological characteristics of dopamine-immunoreactive neurons in the midbrain of the squirrel monkey (Saimiri sciureus). J Comp Neurol. 1988; 267:489–506. [PubMed: 3346372]

Bennett BD, Bolam JP. Characterization of calretinin-immunoreactive structures in the striatum of the rat. Brain Res. 1993; 609:137–148. [PubMed: 8508297]

Bennett BD, Bolam JP. Localisation of parvalbumin-immunoreactive structures in primate caudate-putamen. J Comp Neurol. 1994; 347:340–356. [PubMed: 7822489]

Bernier PJ, Vinet J, Cossette M, Parent A. Characterization of the subventricular zone of the adult human brain: evidence for the involvement of Bcl-2. Neurosci Res. 2000; 37:67–78. [PubMed: 10802345]

Betarbet R, Turner R, Chockkan V, DeLong MR, Allers KA, Walters J, Levey AI, Greenamyre JT. Dopaminergic neurons intrinsic to the primate striatum. J Neurosci. 1997; 17:6761–6768. [PubMed: 9254687]

Bezard E, Gross CE. Compensatory mechanisms in experimental and human parkinsonism: towards a dynamic approach. Prog Neurobiol. 1998; 55:93–116. [PubMed: 9618745]

Bezard E, Gross CE, Brotchie JM. Presymptomatic compensation in Parkinson's disease is not dopamine-mediated. Trends Neurosci. 2003; 26:215–221. [PubMed: 12689773]

Burns RS, Chiueh CC, Markey SP, Ebert MH, Jacobowitz DM, Kopin IJ. A primate model of parkinsonism: selective destruction of dopaminergic neurons in the pars compacta of the substantia nigra by N-methyl-4- phenyl-1,2,3,6-tetrahydropyridine. Proc Natl Acad Sci USA. 1983; 80:4546–4550. [PubMed: 6192438]

Cameron HA, Woolley CS, McEwen BS, Gould E. Differentiation of newly born neurons and glia in the dentate gyrus of the adult rat. Neuroscience. 1993; 56:337–344. [PubMed: 8247264]

Campbell KJ, Takada M, Hattori T. Co-localization of tyrosine hydroxylase and glutamate decarboxylase in a subpopulation of single nigrotectal projection neurons. Brain Res. 1991; 558:239–244. [PubMed: 1685932]

Chang HT, Kita H. Interneurons in the rat striatum: relationships between parvalbumin neurons and cholinergic neurons. Brain Res. 1992; 574:307–311. [PubMed: 1638402]

Cossette M, Bedard A, Parent A. Dopaminergic Neurons in Human Striatum and Neurogenesis in Adult Monkey Striatum. Ann N Y Acad Sci. 2003; 991:346–349.

Cossette M, Parent A, Levesque D. Tyrosine hydroxylase-positive neurons intrinsic to the human striatum express the transcription factor Nurr1. Eur J Neuroscience. 2004; 20:2089–2095.

Cossette M, Lecomte F, Parent A. Morphology and distribution of dopaminergic neurons intrinsic to the human striatum. J Chem Neuroanat. 2005; 29:1–11. [PubMed: 15589697]

Descarries L, Mechawar N. Ultrastructural evidence for diffuse transmission by monoamine and acetylcholine neurons of the central nervous system. Prog Brain Res. 2000; 125:27–47. [PubMed: 11098652]

Descarries L, Watkins KC, Garcia S, Bosler O, Doucet G. Dual character, asynaptic and synaptic, of the dopamine innervation in adult rat neostriatum: a quantitative autoradiographic and immunocytochemical analysis. J Comp Neurol. 1996; 375:167–186. [PubMed: 8915824]

Diaz-Rios M, Oyola E, Miller MW. Colocalization of gamma-aminobutyric acid-like immunoreactivity and catecholamines in the feeding network of Aplysia californica. J Comp Neurol. 2002; 445:29–46. [PubMed: 11891652]

DiFiglia M. Synaptic organization of cholinergic neurons in the monkey neostriatum. J Comp Neurol. 1987; 255:245–258. [PubMed: 3819015]

Difiglia M, Pasik T, Pasik P. Ultrastructure of Golgi-impregnated and gold-toned spiny and aspiny neurons in the monkey neostriatum. J Neurocytol. 1980; 9:471–492. [PubMed: 6160212]

Doetsch F, Garcia-Verdugo JM, Alvarez-Buylla A. Cellular composition and three-dimensional organization of the subventricular germinal zone in the adult mammalian brain. J Neurosci. 1997; 17:5046–5061. [PubMed: 9185542]

Dubach M, Schmidt R, Kunkel D, Bowden DM, Martin R, German DC. Primate neostriatal neurons containing tyrosine hydroxylase: immunohistochemical evidence. Neurosci Lett. 1987; 75:205–210. [PubMed: 2883616]

Dunker N. Colocalization of serotonin and GABA in retinal neurons of Ichthyophis kohtaoensis (amphibia; Gymnophiona). Anat Embryol (Berl). 1998; 197:69–75. [PubMed: 9462859]

Ehringer H, Hornykiewicz O. Verteilung von noradrenalin und dopamin (3-hydroxytyramin) im gehirn des menschen und ihr verhalten bei erkrankungen des extrapyramidalen systems. Klinische Wochenschrift. 1960:1236–1239. [PubMed: 13726012]

Eriksson PS, Perfilieva E, Bjork-Eriksson T, Alborn AM, Nordborg C, Peterson DA, Gage FH. Neurogenesis in the adult human hippocampus. Nat Med. 1998; 4:1313–1317. [PubMed: 9809557]

Fujiyama F, Fritschy JM, Stephenson FA, Bolam JP. Synaptic localization of GABA(A) receptor subunits in the striatum of the rat. J Comp Neurol. 2000; 416:158–172. [PubMed: 10581463]

Gall CM, Hendry SH, Seroogy KB, Jones EG, Haycock JW. Evidence for coexistence of GABA and dopamine in neurons of the rat olfactory bulb. J Comp Neurol. 1987; 266:307–318. [PubMed: 2891733]

Gould E, Reeves AJ, Fallah M, Tanapat P, Gross CG, Fuchs E. Hippocampal neurogenesis in adult Old World primates. Proc Natl Acad Sci USA. 1999a; 96:5263–5267. [PubMed: 10220454]

Gould E, Reeves AJ, Graziano MS, Gross CG. Neurogenesis in the neocortex of adult primates. Science. 1999b; 286:548–552. [PubMed: 10521353]

Harris KM, Kater SB. Dendritic spines: cellular specializations imparting both stability and flexibility to synaptic function. Ann Rev Neurosci. 1994; 17:341–371. [PubMed: 8210179]

Heikkila RE, Hess A, Duvoisin RC. Dopaminergic neurotoxicity of 1-methyl-4-phenyl-1,2,5,6-tetrahydropyridine in mice. Science. 1984; 224:1451–1453. [PubMed: 6610213]

Hersch SM, Ciliax BJ, Gutekunst CA, Rees HD, Heilman CJ, Yung KK, Bolam JP, Ince E, Yi H, Levey AI. Electron microscopic analysis of D1 and D2 dopamine receptor proteins in the dorsal striatum and their synaptic relationships with motor corticostriatal afferents. J Neurosci. 1995; 15:5222–5237. [PubMed: 7623147]

Hornykiewicz O, Kish SJ. Biochemical pathophysiology of Parkinson's disease. Adv Neurol. 1987; 45:19–34. [PubMed: 2881444]

Ingham CA, Hood SH, Taggart P, Arbuthnott GW. Plasticity of synapses in the rat neostriatum after unilateral lesion of the nigrostriatal pathway. J Neurosci. 1998; 18:4732–4743. [PubMed: 9614247]

Isaacson JS, Solis JM, Nicoll RA. Local and diffuse synaptic actions of GABA in the hippocampus. Neuron. 1993; 10:165–175. [PubMed: 7679913]

Kawaguchi Y, Wilson CJ, Augood SJ, Emson PC. Striatal interneurones: chemical, physiological and morphological characterization. Trends Neurosci. 1995; 18:527–535. [PubMed: 8638293]

Kish SJ, Shannak K, Hornykiewicz O. Uneven pattern of dopamine loss in the striatum of patients with idiopathic Parkinson's disease. Pathophysiologic and clinical implications. N Engl J Med. 1988; 318:876–880. [PubMed: 3352672]

Langston JW, Ballard P, Tetrud JW, Irwin I. Chronic Parkinsonism in humans due to a product of meperidine-analog synthesis. Science. 1983; 219:979–980. [PubMed: 6823561]

Lapper SR, Smith Y, Sadikot AF, Parent A, Bolam JP. Cortical input to parvalbumin-immunoreactive neurones in the putamen of the squirrel monkey. Brain Res. 1992; 580:215–224. [PubMed: 1504801]

Lavoie B, Smith Y, Parent A. Dopaminergic innervation of the basal ganglia in the squirrel monkey as revealed by tyrosine hydroxylase immunohistochemistry. J Comp Neurol. 1989; 289:36–52. [PubMed: 2572613]

Levin BE, Katzen HL. Early cognitive changes and nondementing behavioral abnormalities in Parkinson's disease. Adv Neurol. 1995; 65:85–95. [PubMed: 7872154]

Liu F, Wan Q, Pristupa ZB, Yu XM, Wang YT, Niznik HB. Direct protein-protein coupling enables cross-talk between dopamine D5 and gamma-aminobutyric acid A receptors. Nature. 2000; 403:274–280. [PubMed: 10659839]

Lopez-Real A, Rodriguez-Pallares J, Guerra MJ, Labandeira-Garcia JL. Localization and functional significance of striatal neurons immunoreactive to aromatic L-amino acid decarboxylase or tyrosine hydroxylase in rat Parkinsonian models. Brain Res. 2003; 969:135–146. [PubMed: 12676374]

Mazloom M, Smith Y. Ultrastructural characterization of intrastriatal dopaminergic neurons in MPTP-treated monkeys. Soc for Neurosci. 2001; 27:292.9.

Meredith GE, Farrell T, Kellaghan P, Tan Y, Zahm DS, Totterdell S. Immunocytochemical characterization of catecholaminergic neurons in the rat striatum following dopamine-depleting lesions. Eur J Neurosci. 1999; 11:3585–3596. [PubMed: 10564366]

Morello M, Reiner A, Sancesario G, Karle EJ, Bernardi G. Ultrastructural study of nitric oxide synthase-containing striatal neurons and their relationship with parvalbumin-containing neurons in rats. Brain Res. 1997; 776:30–39. [PubMed: 9439793]

Mura A, Jackson D, Manley MS, Young SJ, Groves PM. Aromatic L-amino acid decarboxylase immunoreactive cells in the rat striatum: a possible site for the conversion of exogenous L-DOPA to dopamine. Brain Res. 1995; 704:51–60. [PubMed: 8750961]

Nguyen-Legros J, Versaux-Botteri C, Savy C. Dopaminergic and GABAergic retinal cell populations in mammals. Microsc Res Tech. 1997; 36:26–42. [PubMed: 9031259]

O'Byrne MB, Bolam JP, Hanley JJ, Tipton KF. Tyrosine-hydroxylase immunoreactive cells in the rat striatum following treatment with MPP+ Adv Exp Med Biol. 2000; 483:369–374. [PubMed: 11787621]

Palfi S, Leventhal L, Chu Y, Ma SY, Emborg M, Bakay R, Deglon N, Hantraye P, Aebischer P, Kordower JH. Lentivirally delivered glial cell line-derived neurotrophic factor increases the number of striatal dopaminergic neurons in primate models of nigrostriatal degeneration. J Neurosci. 2002; 22:4942–4954. [PubMed: 12077191]

Parent A. Extrinsic connections of the basal ganglia. Trends Neurosci. 1990; 13:254–258. [PubMed: 1695399]

Parent JM, Vexler ZS, Gong C, Derugin N, Ferriero DM. Rat forebrain neurogenesis and striatal neuron replacement after focal stroke. Ann Neurol. 2002; 52:802–813. [PubMed: 12447935]

Paxinos, G.; Huang, X-F.; Toga, AW. The rhesus monkey brain in stereotaxic coordinates. Academic Press; San Diego: 2000.

Phend KD, Weinberg RJ, Rustioni A. Techniques to optimize post-embedding single and double staining for amino acid neurotransmitters. J Histochem Cytochem. 1992; 40:1011–1020. [PubMed: 1376741]

Pickel VM. Extrasynaptic distribution of monoamine transporters and receptors. Prog Brain Res. 2000; 125:267–276. [PubMed: 11098663]

Porritt MJ, Batchelor PE, Hughes AJ, Kalnins R, Donnan GA, Howells DW. New dopaminergic neurons in Parkinson's disease striatum. Lancet. 2000; 356:44–45. [PubMed: 10892768]

Prensa L, Gimenez-Amaya JM, Parent A. Morphological features of neurons containing calcium-binding proteins in the human striatum. J Comp Neurol. 1998; 390:552–563. [PubMed: 9450535]

Rakic P. Neurogenesis in adult primate neocortex: an evaluation of the evidence. Nat Rev Neurosci. 2002; 3:65–71. [PubMed: 11823806]

Resibois A, Rogers JH. Calretinin in rat brain: an immunohistochemical study. Neuroscience. 1992; 46:101–134. [PubMed: 1594096]

Reynolds ES. The use of lead citrate at high pH as an electron opaque stain in electron microscopy. J Cell Biol. 1963; 17:208–212. [PubMed: 13986422]

Rice ME. Distinct regional differences in dopamine-mediated volume transmission. Prog Brain Res. 2000; 125:277–290. [PubMed: 11098664]

Rudkin TM, Sadikot AF. Thalamic input to parvalbumin-immunoreactive GABAergic interneurons: organization in normal striatum and effect of neonatal decortication. Neuroscience. 1999; 88:1165–1175. [PubMed: 10336127]

Rusakov DA, Lehre KP. Perisynaptic asymmetry of glia: new insights into glutamate signalling. Trends Neurosci. 2002; 25:492–494. [PubMed: 12220870]

Sadikot AF, Parent A, Francois C. Efferent connections of the centromedian and parafascicular thalamic nuclei in the squirrel monkey: a PHA-L study of subcortical projections. J Comp Neurol. 1992a; 315:137–159. [PubMed: 1372010]

Sadikot AF, Parent A, Smith Y, Bolam JP. Efferent connections of the centromedian and parafascicular thalamic nuclei in the squirrel monkey: a light and electron microscopic study of the thalamostriatal projection in relation to striatal heterogeneity. J Comp Neurol. 1992b; 320:228–242. [PubMed: 1619051]

Schneider JS, Kovelowski CJ II. Chronic exposure to low doses of MPTP. I. Cognitive deficits in motor asymptomatic monkeys. Brain Res. 1990; 519:122–128. [PubMed: 2397401]

Schulman H. Nitric oxide: a spatial second messenger. Mol Psychiatry. 1997; 2:296–299. [PubMed: 9246669]

Schwaller B, Buchwald P, Blumcke I, Celio MR, Hunziker W. Characterization of a polyclonal antiserum against the purified human recombinant calcium-binding protein calretinin. Cell Calcium. 1993; 14:639–648. [PubMed: 8242719]

Sesack SR, Aoki C, Pickel VM. Ultrastructural localization of D2 receptor-like immunoreactivity in midbrain dopamine neurons and their striatal targets. J Neurosci. 1994; 14:88–106. [PubMed: 7904306]

Sidibe M, Smith Y. Thalamic inputs to striatal interneurons in monkeys: synaptic organization and co-localization of calcium binding proteins. Neuroscience. 1999; 89:1189–1208. [PubMed: 10362307]

Smith Y, Kieval JZ. Anatomy of the dopamine system in the basal ganglia. Trends Neurosci. 2000; 23:S28–33. [PubMed: 11052217]

Somogyi P, Hodgson AJ, Chubb IW, Penke B, Erdei A. Antisera to gamma-aminobutyric acid. II. Immunocytochemical application to the central nervous system. J Histochem Cytochem. 1985; 33:240–248. [PubMed: 2579123]

Song DD, Haber SN. Striatal responses to partial dopaminergic lesion: Evidence for compensatory sprouting. J Neurosci. 2000; 20:5102–5114. [PubMed: 10864967]

Stanic D, Parish CL, Zhu WM, Krstew EV, Lawrence AJ, Drago J, Finkelstein DI, Horne MK. Changes in function and ultrastructure of striatal dopaminergic terminals that regenerate following partial lesions of the SNpc. J Neurochem. 2003; 86:329–343. [PubMed: 12871574]

Stanic D, Finkelstein DI, Bourke DW, Drago J, Horne MK. Time course of striatal reinnervation following lesions of dopaminergic SNpc neurons of the rat. Eur J Neurosci. 2003; 18:1175–1188. [PubMed: 12956716]

Szelenyi J. Cytokines and the central nervous system. Brain Res Bull. 2001; 54:329–338. [PubMed: 11306183]

Tashiro Y, Kaneko T, Sugimoto T, Nagatsu I, Kikuchi H, Mizuno N. Striatal neurons with aromatic L-amino acid decarboxylase-like immunoreactivity in the rat. Neurosci Lett. 1989a; 100:29–34. [PubMed: 2761778]

Tashiro Y, Sugimoto T, Hattori T, Uemura Y, Nagatsu I, Kikuchi H, Mizuno N. Tyrosine hydroxylase-like immunoreactive neurons in the striatum of the rat. Neurosci Lett. 1989b; 97:6–10. [PubMed: 2563908]

Thomas TM, Smith Y, Levey AI, Hersch SM. Cortical inputs to m2-immunoreactive striatal interneurons in rat and monkey. Synapse. 2000; 37:252–261. [PubMed: 10891862]

Ungerstedt U. 6-Hydroxy-dopamine induced degeneration of central monoamine neurons. Eur J Pharmacol. 1968; 5:107–110. [PubMed: 5718510]

Vizi ES. Role of high-affinity receptors and membrane transporters in nonsynaptic communication and drug action in the central nervous system. Pharmacol Rev. 2000; 52:63–89. [PubMed: 10699155]

Vizi ES, Kiss JP. Neurochemistry and pharmacology of the major hippocampal transmitter systems: synaptic and nonsynaptic interactions. Hippocampus. 1998; 8:566–607. [PubMed: 9882017]

Vuillet J, Dimova R, Nieoullon A, Goff LK. Ultrastructural relationships between choline acetyltransferase- and neuropeptide y-containing neurons in the rat striatum. Neuroscience. 1992; 46:351–360. [PubMed: 1542411]

Watts, RL.; Koller, WC. Movement disorders : neurologic principles and practice. McGraw-Hill Health Professions Division; New York: 1997.

Wolf ME, Kapatos G. Flow cytometric analysis and isolation of permeabilized dopamine nerve terminals from rat striatum. J Neurosci. 1989; 9:106–114. [PubMed: 2563275]

Wu Y, Parent A. Striatal interneurons expressing calretinin, parvalbumin or NADPH-diaphorase: A comparative study in the rat, monkey and human. Brain Res. 2000; 863:182–191. [PubMed: 10773206]

Yang M, Stull ND, Berk MA, Snyder EY, Iacovitti L. Neural stem cells spontaneously express dopaminergic traits after transplantation into the intact or 6-hydroxydopaminelesioned rat. Exp Neurol. 2002; 177:50–60. [PubMed: 12429210]

Yung KK, Bolam JP, Smith AD, Hersch SM, Ciliax BJ, Levey AI. Immunocytochemical localization of D1 and D2 dopamine receptors in the basal ganglia of the rat: light and electron microscopy. Neuroscience. 1995; 65:709–730. [PubMed: 7609871]

Zoli M, Agnati LF. Wiring and volume transmission in the central nervous system: the concept of closed and open synapses. Prog Neurobiol. 1996; 49:363–380. [PubMed: 8888115]

Zoli M, Jansson A, Sykova E, Agnati LF, Fuxe K. Volume transmission in the CNS and its relevance for neuropsychopharmacology. Trends Pharmacol Sci. 1999; 20:142–150. [PubMed: 10322499]

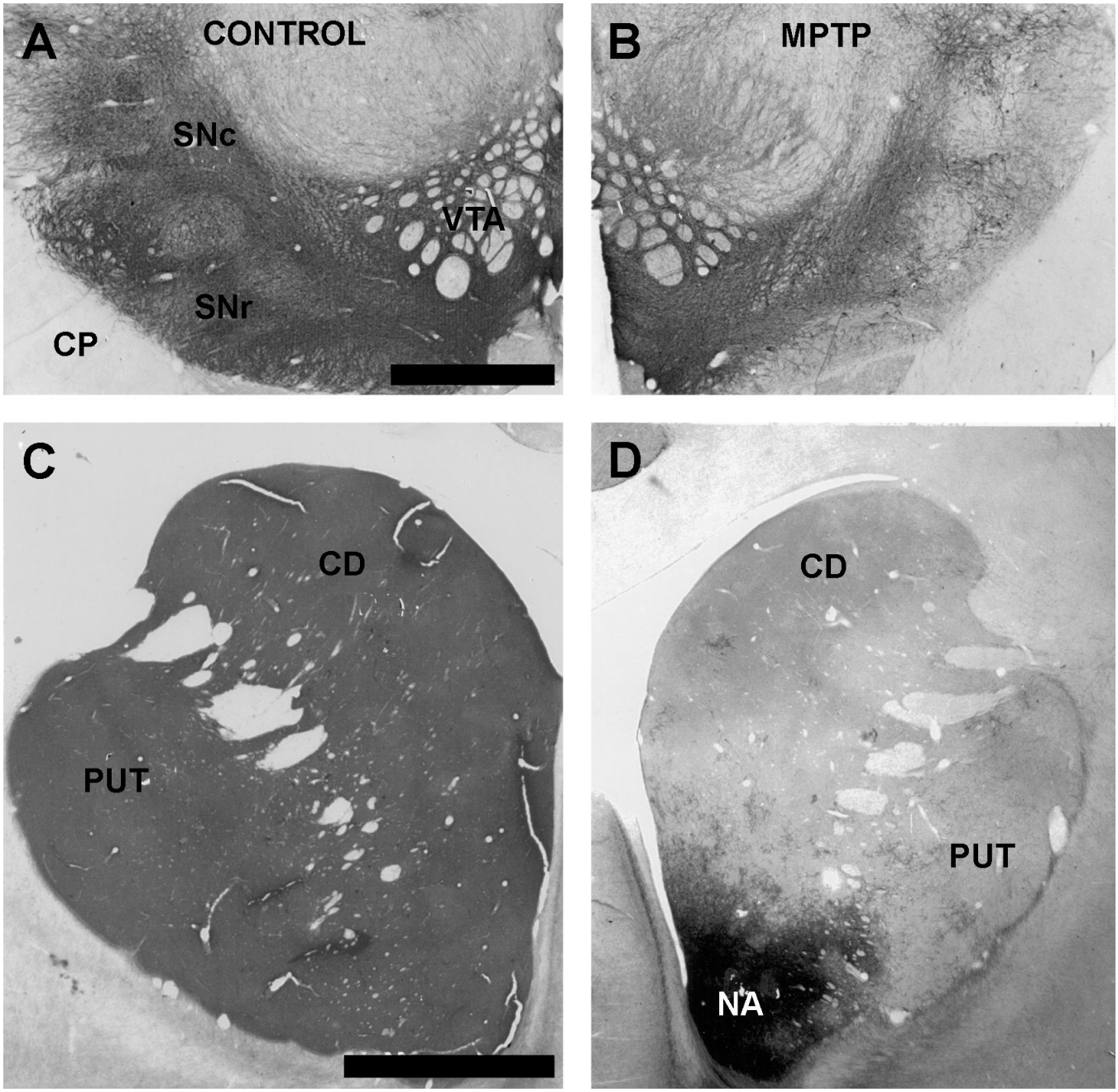

Figure 1.

Light micrographs of TH immunoreactivity in the substantia nigra (A, B) and striatum (C, D) on the contralateral (A, C) and MPTP-treated (B, D) sides of a unilaterally lesioned monkey. Note the massive loss of dopaminergic innervation of the dorsal striatum on the MPTP-lesioned side (D) compared to the control side (C). Abbreviations: Cerebral peduncle (CP), caudate nucleus (CD), nucleus accumbens (NA), putamen (PUT), substantia nigra pars compacta (SNc), substantia nigra pars reticulata (SNr), ventral tegmental area (VTA). Scale bars: (A) 2 mm, applies to B. (C) 2 mm, applies to D.

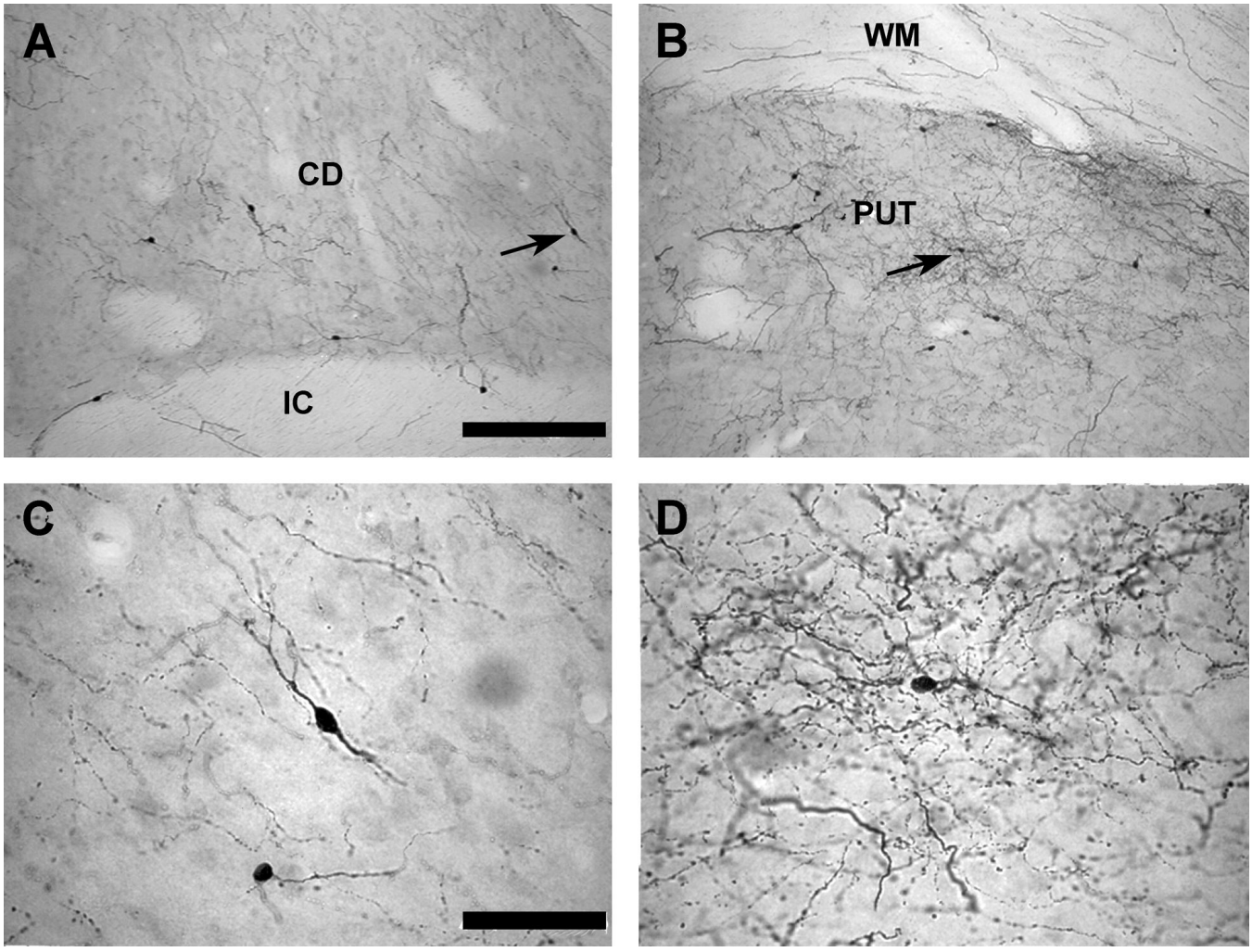

Figure 2.

Light micrographs of TH-containing neuronal cell bodies and processes in the striatum of MPTP-treated monkeys. (A, B) Low power (10x) view of the dorsal borders of the caudate (CD) and putamen (PUT) showing intrastriatal TH-ir neuronal cell bodies and processes. Note TH-immunoreactive fibers in the overlying white matter (WM) and internal capsule (IC). Arrows in A and B indicate regions depicted at high magnification in C and D, respectively. (C) High power (40x) view of two TH-ir cells in the caudate nucleus. Note the small cell body and aspiny characteristic of the dendritic processes. (D) High power view of a TH-ir neuronal perikaryon embedded in a rich field of varicose processes in the putamen. Scale bars: (A) 200 μm, applies to B. (C) 50 μm, applies to D.

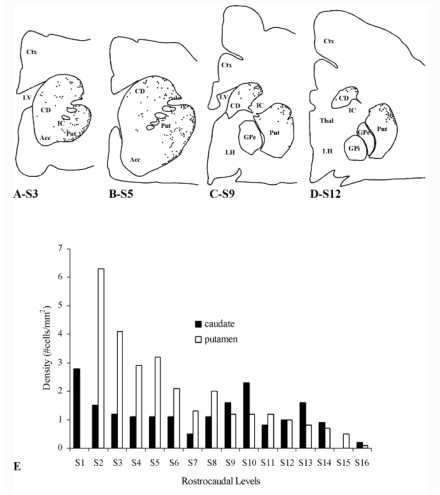

Figure 3.

Distribution of TH-ir cell profiles through the rostrocaudal extent of the striatum in a unilateral MPTP-treated monkey. (Top) Schematic diagram of four sections taken at various rostrocaudal levels of the striatum showing the localization and relative densities of intrastriatal TH-ir cell body profiles. The numbering of the section corresponds to their relative rostrocaudal level according to the atlas of Paxinos et al. (2000); S3=AP +26.85; S5=AP +25.05, S9=AP +16.95, S12=AP +14.25. (Bottom) Histogram illustrating the relative density of TH-ir cell profiles through the rostrocaudal extent of the caudate nucleus and putamen. Note that the caudate nucleus is labeled quite homogeneously along its entire extent whereas neurons in the putamen are predominantly localized in the rostral, pre-commissural part of the structure.

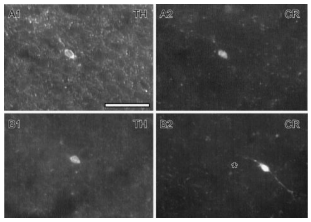

Figure 4.
Co-localization study of TH (A1,B1; TRITC-labeled) and CR (A2,B2; FITC-labeled) in striatal neurons. (A1,A2) show an example of a double labeled neuron; (B1) shows a TH-positive neuronal cell body devoid of CR immunoreactivity (B2). The star in B2 corresponds to the location of the TH-positive neuron in B1. A CR-containing neuron, non-immunoreactive for TH is shown in B2. Scale bar: 50 μm.

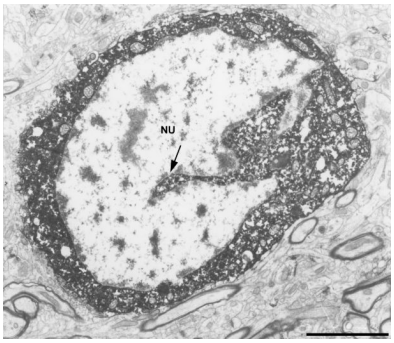

Figure 5.
Electron micrograph of a TH-immunoreactive perikaryon. Note the intense peroxidase labeling of the cytoplasm. The arrow indicates the nuclear invagination, a common ultrastructural feature of striatal interneurons. Nucleus (NU). Scale bar: 3μm.

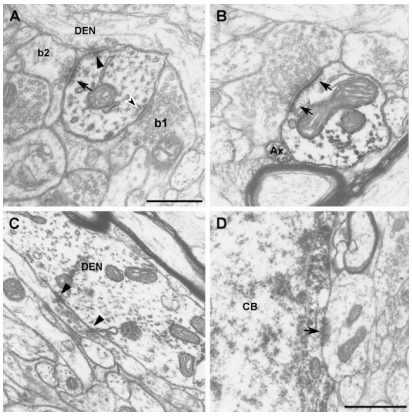

Figure 6.

Synaptic inputs to TH-ir neurons. (A) A TH-positive dendrite receiving a symmetric (open arrow) and an asymmetric (arrow) synapse from two morphologically distinct types of axon terminals (b1, b2). Note also the apposition with an unlabeled dendrite (DEN) (arrowhead). (B) A TH-ir dendrite forming an asymmetric synapse (arrow) with a type of terminal, ultrastructurally different from b2 in A. Note the TH-ir unmyelinated axon (Ax) near the dendrite. (C) A TH-ir dendrite forming two symmetric *en passant* type synapses with a vesicle-filled axonal profile (arrowheads). Note that vesicles in the axon are confined to the site of synaptic contact. (D) A TH-ir cell body (CB) forming an asymmetric synapse with an unlabeled bouton ultrastructurally different from those shown in A and B. This is the only axo-somatic synapse seen on the 14 TH-containing perikarya examined in this study. Scale bars: (A) 0.5μm, applies to B and C. (D) 1μm.

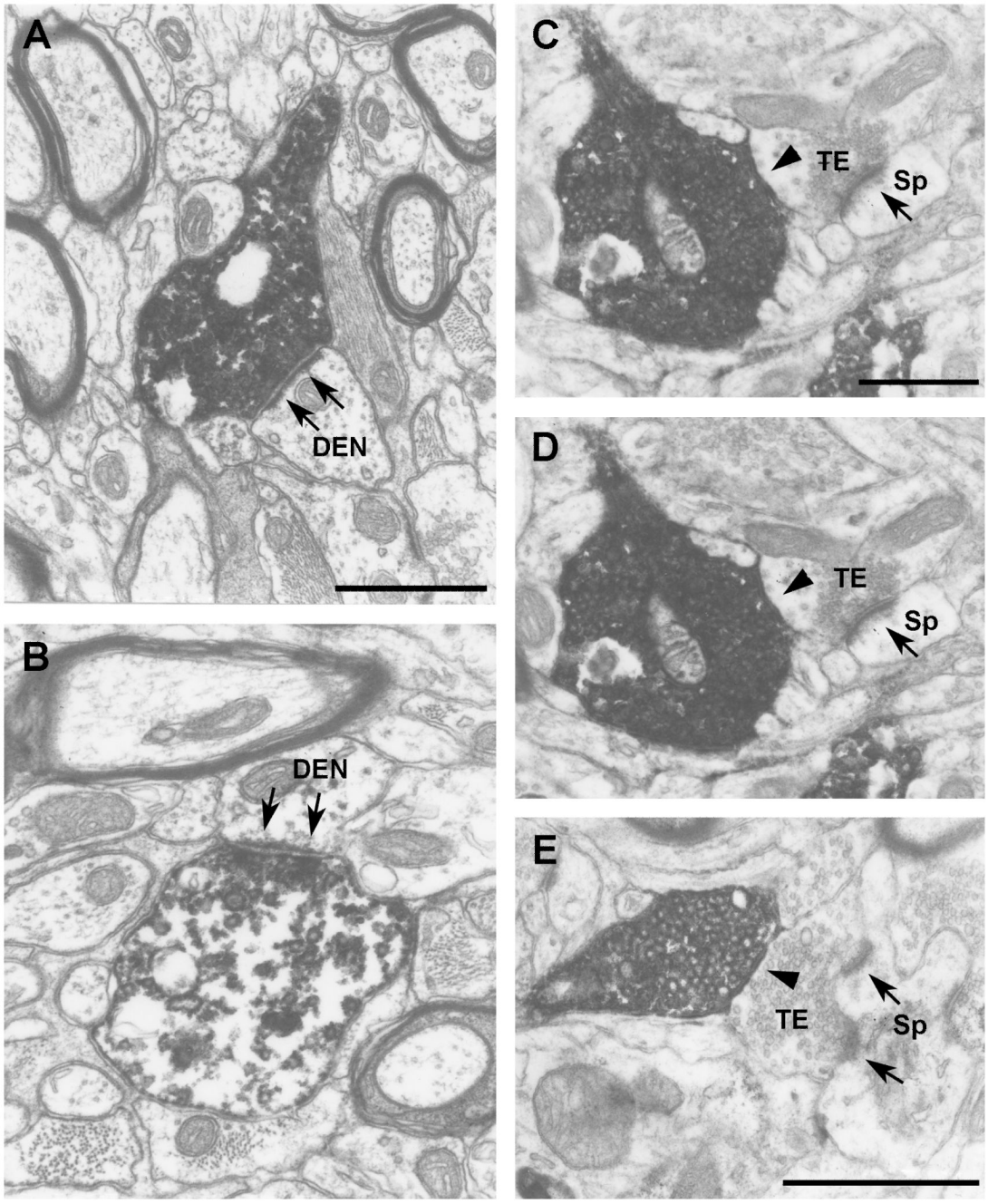

Figure 7.
Synaptic connectivity of TH-ir terminals. (A,B) TH-ir terminals forming asymmetric synapses (arrows) onto small dendrites (DEN). Note that the postsynaptic dendrite in B displays light TH immunoreactivity. (C-E) Examples of TH-ir terminals apposed (open arrows) to unlabeled terminals (TE), forming asymmetric synapses (arrows) with unlabeled spines (Sp). Note that C and D are serial sections of the same TH-ir terminal. Scale bars: (A) 1μm, applies to B; (C) 1 μm, applies to D; (E) 2 μm.

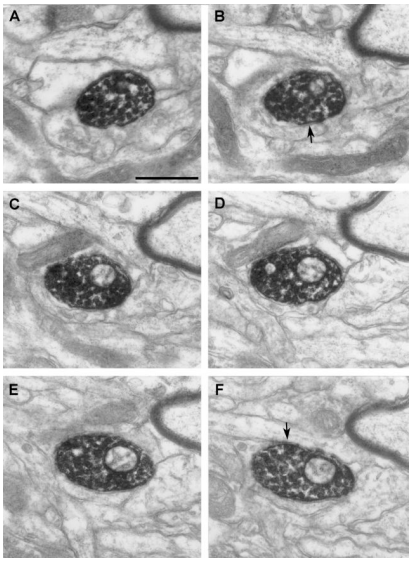

Figure 8.
Serial sections of a vesicle-filled TH-ir terminal. This represents the most common type of TH-containing terminal structure seen in the striatum of MPTP-treated monkeys. Arrows in B, D, and F indicate sites of appositions between the labeled profile and unlabeled structures. Scale bar: (A) 0.5 μm applies to B-F.

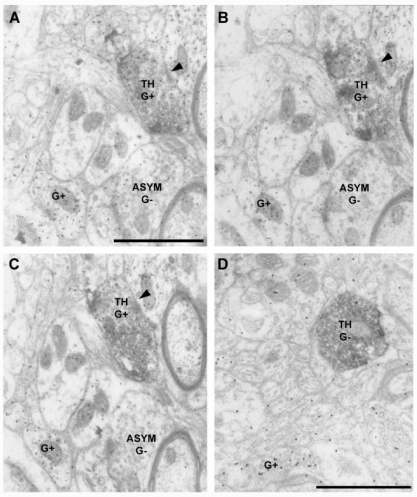

Figure 9.
GABA immunoreactivity in intrastriatal TH-ir terminals. (A-C) Serial sections of a TH-ir terminal displaying GABA immunoreactivity (TH, G+). In the same micrographs, a terminal forming an asymmetric axo-spinous synapse (ASYM, G-) contains a much lower density of gold particles than the TH-positive bouton and a putative GABAergic, TH-negative, terminal (G+). (D) A TH-ir/GABA-negative terminal (TH, G-) within the striatum of a normal monkey. Note the difference in gold particle density associated with the TH-positive terminal and a putative GABA-containing bouton in the same field (G+). Scale bars: (A) 1 μm, applies to B, C; 1 μm in D.

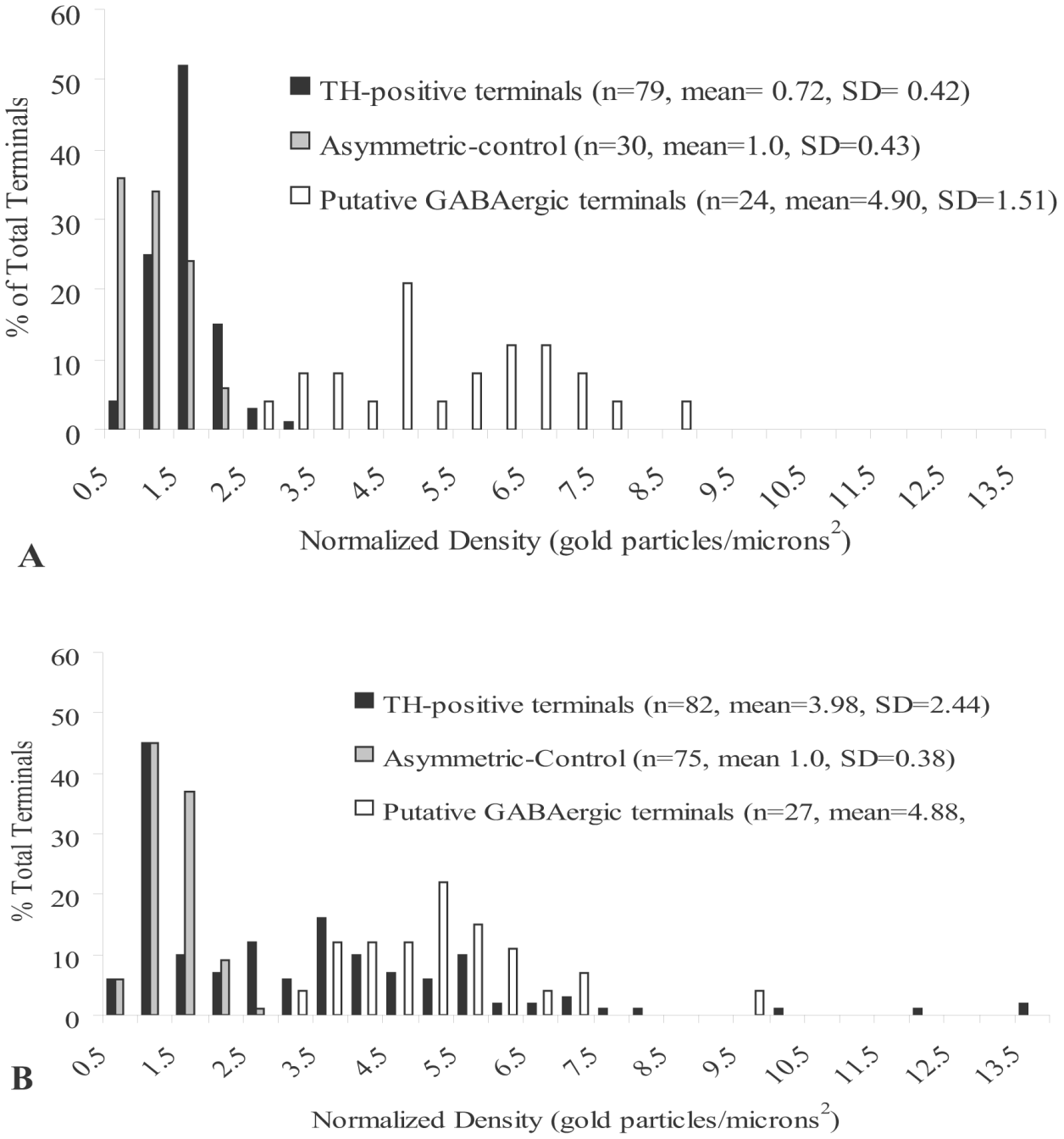

Figure 10.

Histograms showing the relative density of gold particles associated with TH-ir terminals in two normal (A) and four MPTP-treated (B) monkeys. TH-negative terminals forming asymmetric (putative glutamatergic) or symmetric (putative GABAergic) synapses were used as controls for the specificity of gold labeling. The mean and standard deviation of gold particle densities for each population of terminals examined is given in parentheses.

Table 1

Synaptic inputs onto TH-immunoreactive dendrites

Diameter elements	# elements observed	# asymmetric synapses	# symmetric synapses	# unknown synapses
> **1.0 μm**	183	20	8	7
0.5-1.0 μm	22	2	0	0
< **0.5 μm**	0	0	0	0

Table 2

Length of synapses onto TH-immunoreactive dendrites

Diameter of elements (μm)	Total length of dendrites (μm)	Total length of asymmetric synapses (μm)	Total length of symmetric synapses (μm)	Total length of unknown synapses (μm)
>**1.0 μm**	1059.46	8.33 (0.8%)	1.96 (0.2%)	1.72 (0.2%)
0.5-1.0 μm	58.54	0.93 (1.5%)	0	0

The percentages are fraction of total dendritic length obsereved.